Featured in Physics

Superconductivity from On-Chip Metallization on 2D Topological Chalcogenides

Yanyu Jia,[1,*] Guo Yu,[1,2] Tiancheng Song,[1] Fang Yuan,[3] Ayelet J. Uzan,[1] Yue Tang,[1] Pengjie Wang,[1] Ratnadwip Singha,[3] Michael Onyszczak,[1] Zhaoyi Joy Zheng,[1,2] Kenji Watanabe,[4] Takashi Taniguchi,[5] Leslie M. Schoop,[3] and Sanfeng Wu[1,†]

[1]*Department of Physics, Princeton University, Princeton, New Jersey 08544, USA*
[2]*Department of Electrical and Computer Engineering, Princeton University, Princeton, New Jersey 08544, USA*
[3]*Department of Chemistry, Princeton University, Princeton, New Jersey 08544, USA*
[4]*Research Center for Electronic and Optical Materials, National Institute for Materials Science, 1-1 Namiki, Tsukuba 305-0044, Japan*
[5]*Research Center for Materials Nanoarchitectonics, National Institute for Materials Science, 1-1 Namiki, Tsukuba 305-0044, Japan*

(Received 19 December 2023; revised 3 March 2024; accepted 25 April 2024; published 21 June 2024)

Two-dimensional (2D) transition metal dichalcogenides (TMDs) is a versatile class of quantum materials of interest to various fields including, e.g., nanoelectronics, optical devices, and topological and correlated quantum matter. Tailoring the electronic properties of TMDs is essential to their applications in many directions. Here, we report that a highly controllable and uniform on-chip 2D metallization process converts a class of atomically thin TMDs into robust superconductors, a property belonging to none of the starting materials. As examples, we demonstrate the introduction of superconductivity into a class of 2D air-sensitive topological TMDs, including monolayers of T_d-WTe_2, 1T′-$MoTe_2$, and 2H-$MoTe_2$, as well as their natural and twisted bilayers, metallized with an ultrathin layer of palladium. This class of TMDs is known to exhibit intriguing topological phases ranging from topological insulator, Weyl semimetal to fractional Chern insulator. The unique, high-quality two-dimensional metallization process is based on our recent findings of the long-distance, non-Fickian in-plane mass transport and chemistry in 2D that occur at relatively low temperatures and in devices fully encapsulated with inert insulating layers. Highly compatible with existing nanofabrication techniques for van der Waals stacks, our results offer a route to designing and engineering superconductivity and topological phases in a class of correlated 2D materials.

DOI: 10.1103/PhysRevX.14.021051

Subject Areas: Condensed Matter Physics, Strongly Correlated Materials, Topological Insulators

I. INTRODUCTION

Introducing and designing superconductivity in non-superconducting quantum materials are often desired for engineering new phases of matter and superconducting (SC) quantum devices. A prominent example is the hope to create non-Abelian anyons in artificial nanostructures [1–3]. For instance, introducing superconductivity to a topological insulator has been proposed for realizing the long-sought-after Majorana zero modes [3–5], an Ising type of anyons that can be used for demonstrating non-Abelian braiding statistics and partial operations of a topological quantum bit. In more ambitious theoretical proposals combining superconductivity and fractional quantum Hall edge states, one may in principle realize distinct types of non-Abelian states, such as the parafermion modes [2,6–9], which could achieve full operations of a topological quantum bit. However, many proposals require high-quality designable integration of superconductors with topological quantum materials, representing a key challenge from device engineering perspectives.

Conventional approaches of depositing a superconducting metal to the surface of a material [Fig. 1(a)] have been employed in, e.g., the nanowire [10], quantum well [11], and graphene systems [12], to name a few. However, for a class of air-sensitive two-dimensional (2D) materials, this technique faces severe challenges in producing high-quality devices. Recent studies have shown that superconducting compounds may be created at the contact vicinity between a deposited metal and a layered material

*yanyuj@princeton.edu
†sanfengw@princeton.edu

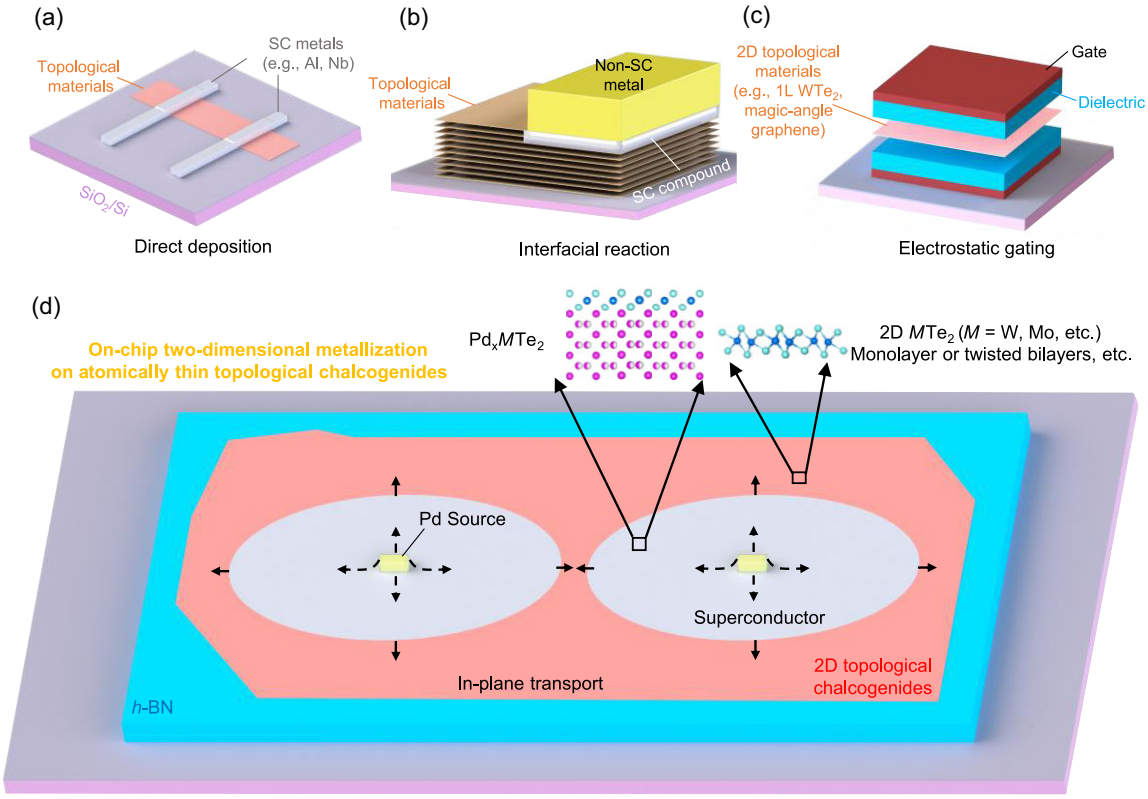

FIG. 1. On-chip two-dimensional metallization on atomically thin topological chalcogenides. (a)–(c) List of known approaches for introducing superconductivity to nonsuperconducting materials, including direct metal deposition of metal superconductors (a) in a large chamber, interfacial reaction that produces superconducting compound at contact (b), and the rare cases of gate-induced superconductivity (c). (d) Our approach of on-chip 2D metallization, based on the recent finding of the long-distance non-Fickian 2D mass transport of Pd at relatively low temperatures (Ref. [27]). The process converts regions of 2D TMDs, e.g., MTe_2 (M = W, Mo), into a new superconducting compound Pd_xMTe_2, in a controllable and designable fashion.

due to interfacial reactions [13–17] [Fig. 1(b)]. The superconducting contact created in this process is, however, nonuniform and of small volume attached to a bulk nonsuperconducting metal. In a study of multilayer WTe_2 Josephson junctions employing this method, an additional superconducting metal was deposited to improve the transport quality of the device [13]. Similar efforts have also been put forward in introducing superconductivity in epitaxy-grown topological insulators [18–21]. Superconductivity at low carrier densities may also be realized by electrostatic gating in novel 2D materials, e.g., monolayer WTe_2 [22,23] and magic-angle graphene systems [24–26] [Fig. 1(c)]. However, these outstanding situations are rare and unlikely to be generalized to the diverse family of 2D quantum materials.

Here, we report the creation of robust superconductivity in a class of 2D transition metal dichalcogenides (TMDs) metallized with a uniform layer of atomically thin palladium. The results are based on our recent surprising finding [27] of a rapid, long-distance, non-Fickian (hence, nondiffusive) in-plane transport of metal films on monolayer TMDs at temperatures well below the melting points of all materials involved. The process realizes on-chip 2D chemical synthesis templated on monolayer crystals [Fig. 1(d)], based on which we demonstrate its capability in introducing superconductivity into 2D materials. We characterize the electronic properties of the resultant new 2D compounds created in topological chalcogenides, including Pd-metallized monolayer and bilayer T_d-WTe_2, monolayer 1T′-$MoTe_2$, monolayer and twisted bilayer 2H-$MoTe_2$, and find superconductivity in all these cases.

II. RESULTS

A. Superconductivity in 2D Pd-metallized WTe_2

WTe_2 monolayer is an excitonic topological insulator exhibiting the quantum spin Hall effect [28–33]. Introducing superconductivity to its helical edge mode is proposed as a route to topological superconductivity and Majorana zero modes [4,5]. Superconductivity has been previously found in monolayer WTe_2 under electrostatic gating [22,23], in which superconducting properties are sensitive to carrier density. Here, we show a distinct approach for introducing superconductivity to monolayer and bilayer WTe_2 based on the on-chip 2D metallization and crystal growth method [27]. The experiments start with

fabricating a van der Waals (vdW) stack consisting of mechanically exfoliated monolayer or bilayer WTe_2 and hexagonal boron nitride (*h*-BN), placed on top of a SiO_2/Si substrate. Inside the stack, Pd seed islands, in contact with WTe_2, are predeposited using standard nanolithography techniques. Upon heating the stack at ~200 °C, a subnanometer-thick layer of Pd transports from the seeds and spreads uniformly over the entire 2D flake in about an hour [Figs. 2(a) and 2(b)]. This anomalous mass transport and the resulting new crystalline compound, with a chemical composition Pd_7WTe_2, were characterized in a previous work [27]. Here, we report the electronic transport properties of the new compound and find that it is a superconductor at ultralow temperatures. It is interesting to note that neither of the starting materials (WTe_2 and Pd) superconduct in their pristine forms.

Figure 2(c) plots the four-probe resistance (R_{xx}) as a function of temperature (T) measured on Pd_7WTe_2 in

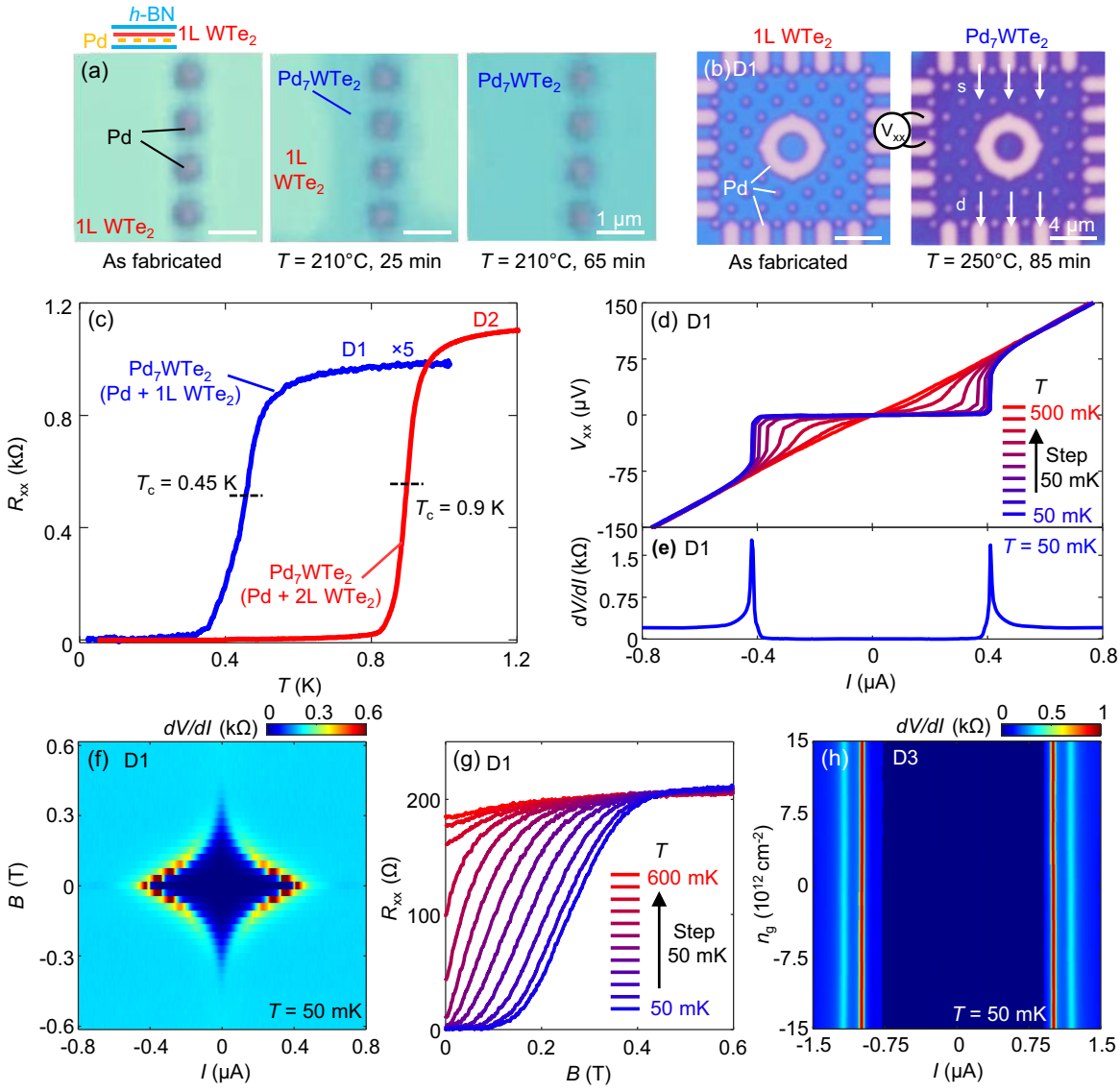

FIG. 2. Superconductivity in Pd_7WTe_2. (a) Optical images of a device demonstrating the on-chip metallization process for a monolayer (1L) WTe_2 placed on top of Pd seeds, encapsulated by *h*-BN. WTe_2 is large and covers the whole imaging window. Left: the device as fabricated. Middle: an image of the device after heat treatment at ~210 °C for 25 min. Right: after 65 min (WTe_2 inside the window is fully converted to Pd_7WTe_2). The characterization of this process and the new Pd_7WTe_2 compound are discussed in Ref. [27]. (b) A similar process for another device (D1), before (left-hand image) and after (right-hand image) the heat treatment. Here, the Pd leads also serve as transport electrodes. (c) R_{xx} of Pd_7WTe_2 measured for D1 (blue, seeded on monolayer WTe_2) and D2 (red, seeded on bilayer WTe_2), as a function of temperature. (d) Nonlinear *IV* curves (top, at different T) and (e) differential resistance dV/dI, as a function of applied dc current I, demonstrating the effect of critical currents. (f) A dV/dI map that reveals the vanishing critical currents under magnetic fields B. (g) R_{xx} as a function of B, taken at various T. (h) dV/dI versus I, taken over the entire gate range in D3 with gate electrodes, revealing no gate dependence.

device D1 (seeded on monolayer WTe_2) and D2 (seeded on bilayer WTe_2). D1 displays a characteristic resistance drop to zero near $T_c \sim 0.45$ K, at which R_{xx} is half of its normal state value. The bilayer seeded Pd_7WTe_2 (D2) exhibits a higher $T_c \sim 0.9$ K. The superconducting nonlinear *IV* curves, as well as differential resistance, are shown in Figs. 2(d) and 2(e), revealing a critical current of ~0.4 μA in this device. A perpendicular magnetic field fully suppresses superconductivity at $B_c \sim 0.4$ T [Figs. 2(f) and 2(g)]. These observations confirm superconductivity in this new compound. We have also fabricated a dual-gated device (D3), in which we can electrostatically vary the electron density n_g in Pd_7WTe_2 by $\sim \pm 1.5 \times 10^{13}$ cm^{-2}. Within this entire range, we find no change in the superconducting properties [Fig. 2(h)], implying a high carrier density in the sample. This is in sharp contrast to the gate-induced low-density superconductivity [22,23] in monolayer WTe_2, which develops a strong insulator state in the absence of gating-induced doping ($n_g \sim 0$) [32]. Also, the critical magnetic field found in Pd_7WTe_2 is much larger than that found in the gate-induced superconductivity [22,23] in intrinsic monolayer WTe_2, further confirming a distinct origin. We further note that in our Pd_7WTe_2 device [D1, Fig. 2(b)] the data are taken when the monolayer WTe_2 is fully converted to Pd_7WTe_2, so there is no longer WTe_2 in the device. The atomic structure of W-Te-W in Pd_7WTe_2 is completely different from the pristine WTe_2 [27]. In Supplemental Material Fig. S1, we characterize the superconducting properties of the bilayer seeded Pd_7WTe_2 (D2) [34]. In Supplemental Material Fig. S2, we show a Fraunhofer-like pattern seen in the critical current measurement, induced by disorders that create an accidental junction, demonstrating the superconducting interference effects. In Supplemental Material Fig. S3, we present the measurement of the vortex Nernst effect that directly signifies the formation and motion of superconducting vortices. These comprehensive characterizations establish superconductivity in the new Pd_7WTe_2 compound.

B. Superconductivity in 2D Pd-metallized 1T′-$MoTe_2$ and 2H-$MoTe_2$

At room temperature, $MoTe_2$ monolayer can be stabilized in two different phases, exhibiting either a monoclinic (1T') or a hexagonal lattice structure (2H). 1T′-$MoTe_2$ is known as a candidate of Weyl semimetal and develops superconductivity below 0.1 K [35,36]. In contrast, 2H-$MoTe_2$ is a semiconductor, not a superconductor. We fabricate both monolayer 1T′-$MoTe_2$ (D4) and monolayer 2H-$MoTe_2$ (D5) in contact with Pd seeds, fully encapsulated with *h*-BN from the top and bottom. When the stack is placed at ~250 °C, Pd rapidly propagates in the 2D plane and reacts with the $MoTe_2$ monolayer flake, just like the Pd transportation on WTe_2. Figures 3(a) and 3(b) display optical microscope images of the two devices (D4 and D5) before and after the heat treatment, revealing the consequence of the Pd metallization. Note that, as we have emphasized previously, the long-distance transport process here must involve chemical affinity between Pd and Te, not a simple physical diffusion. The resulting final material is a new compound Pd_xMoTe_2 consisting of Pd and atoms from the seed monolayers. Atomic force microscopy suggests that the thickness of the new compound is ~1.5 nm and the thickness increases after Pd metallization is ~0.8 nm (Supplemental Material Fig. S4 [34]), close to that of Pd_7WTe_2 obtained in the WTe_2 case, suggesting that x is close to 7 as well in the $MoTe_2$ cases. Further characterizations of the compounds are necessary to uncover their exact atomic structures in these two cases, which we leave for future study.

Here, we focus on the transport properties of the new materials and find that in both cases they superconduct. Figures 3(c)–3(e) plot four-probe resistance measured on a Pd-metallized monolayer 1T′-$MoTe_2$, showing a $T_c \sim 0.45$ K and a $B_c \sim 0.4$ T. Similar values are observed in Pd-metallized monolayer 2H-$MoTe_2$ [Figs. 3(f)–3(h)]. The normal state resistance R_n of these two devices is, however, quite different, being ~800 Ω for D4 whereas ~33 Ω for D5. This could be an indication that the resulting materials in the two cases may not be identical, although the transport device geometry plays a role. Consistent with the normal state resistance, the critical current in D4 ($I_c \sim 100$ nA) is much smaller than that of D5 ($I_c \sim 1$ μA), and consequently I_cR_n does not differ by too much, consistent with the fact that T_c is similar. It is possible that superconductivity resides on the Pd-Te layer formed in the structure. We note that in our high-resolution scanning transmission electron image of the Pd_7WTe_2 compound, no lattice structure can be identified as a single layer of known PdTe or $PdTe_2$ crystals [27]. Another possibility is that the superconductivity resides on the 2D Pd layer. Even though bulk Pd does not superconduct, the ultrathin Pd realized in our case has a unique lattice structure [27] and is possibly a superconductor. Also note that Pd hydrides superconduct, but this is unlikely the situation as our whole fabrication happens within an Ar-filled glovebox. We do not have a conclusion on the exact atomic origin of superconductivity at this point, but conclude that the new compound as whole is a superconductor.

C. Designing superconductivity in a fractional Chern insulator (FCI)

Recently, the fractional quantum anomalous Hall (FQAH) effect, a zero-magnetic field analog of fractional quantum Hall effect expected for fractional Chern insulators (FCIs), has been discovered in bilayer 2H-$MoTe_2$ twisted at an interlayer angle of 3°–4° after a series of experiments at University of Washington that uncovered its magnetism [37], Chern number [38], and the fractionally quantized Hall transport [39]. The thermodynamic evidence [40] and quantized Hall transport [41] of the FCIs in

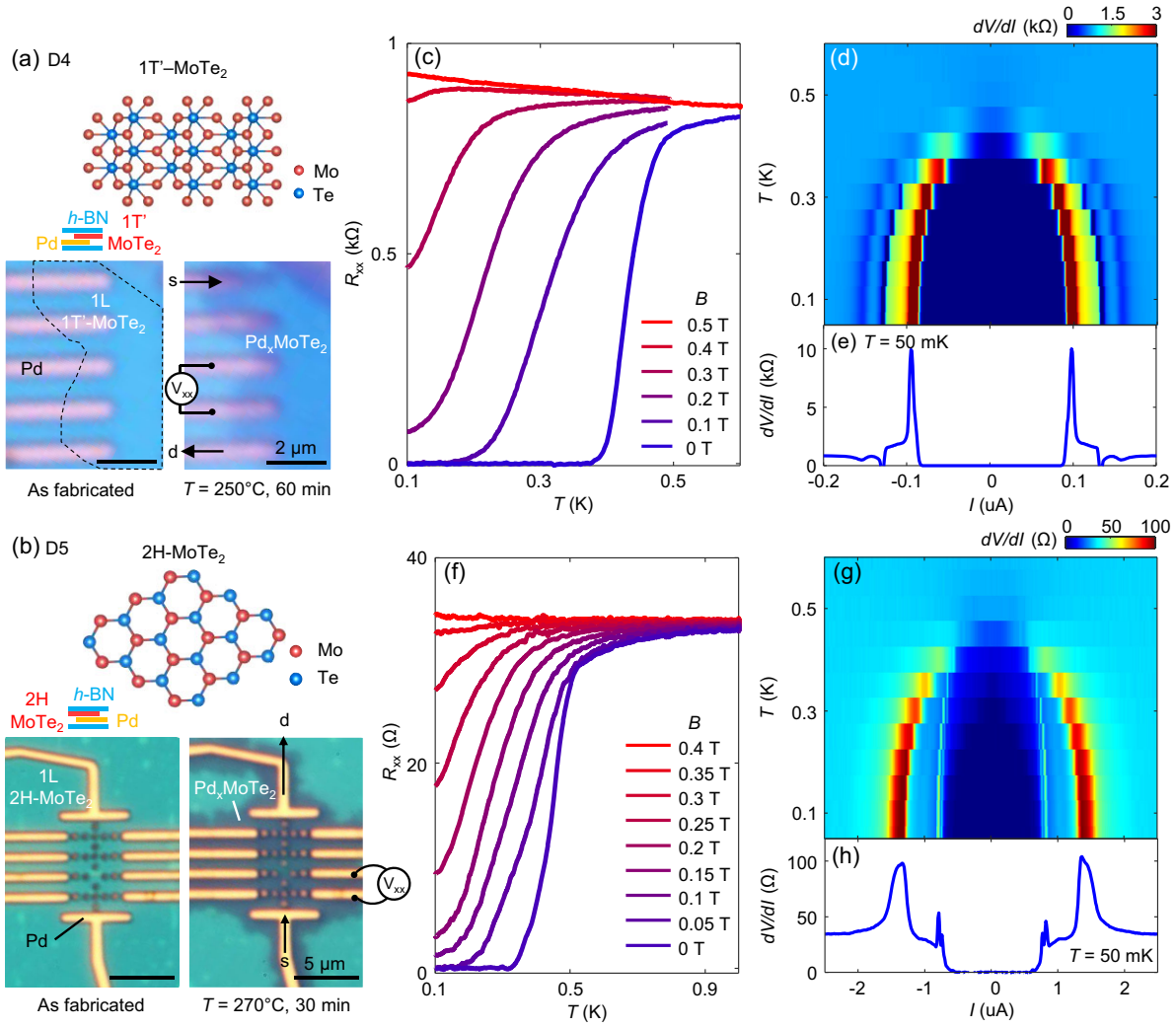

FIG. 3. Superconductivity in Pd_xMoTe_2. (a) Optical images of a device (D4) for Pd metallization on monolayer 1T′-$MoTe_2$, before (left) and after (right) the heat treatment. The crystal structure of 1T′-$MoTe_2$ is shown on the top. With Pd coverage, the monolayer region become darker, signifying the formation of the new compound Pd_xMoTe_2. (b) The same as (a), but for 2H-$MoTe_2$. (c) R_{xx} of Pd_xMoTe_2 as a function of T, taken from D4 at various magnetic fields. (d) dV/dI map under varying I and T. (e) dV/dI versus I at 50 mK. A dip around $\sim \pm 0.13$ μA is seen in (e), featuring a negative dV/dI (note that this is not a negative resistance, but a differential resistance), which signifies a voltage perturbation due to superconducting transition in a neighboring region and hence inhomogeneity in this specific sample. (f)–(h) The dataset for 2D Pd-metallized compound on monolayer 2H-$MoTe_2$ (D5).

the same system have also been reported by two groups at Cornell University and Shanghai Jiao Tong University, respectively. This is an exciting development in the field of topological and correlated phases of matter. One next question is to ask whether there will be interesting new phenomena if superconductivity is introduced to such systems. Theoretically, this could offer a possibility to realize new fractionalized electronics state, such as parafermion modes [2,6–9]. It is not yet known how to introduce superconductivity into this highly interesting but air-sensitive 2D material system. Conventional approaches based on deposition of elemental superconductors are difficult without reducing its quality. Here, we demonstrate that our on-chip 2D Pd metallization introduces superconductivity into twisted bilayer 2H-$MoTe_2$ in a designable fashion.

We fabricate twisted bilayer 2H-$MoTe_2$ (D6) at an angle of ∼3.7° (determined using optical images during fabrication) that favors the FCI states upon electrostatic gating, in contact with predeposited Pd stripes which serve as both the Pd seeds and the electrodes for transport measurement [Fig. 4(a)]. Figures 4(b) and 4(c) show optical microscope images of the device before and after heat treatments at 220 °C for 40 min, during which in-plane Pd transport occurs similarly to previous situations. Note that pristine monolayer and twisted bilayer 2H-$MoTe_2$ are insulators (see Supplemental Material Fig. S5 for characterization of the contact properties before and after a slight Pd transport [34]). With the Pd treatment, the resulting material turns into a metal that develops superconductivity with $T_c \sim 1$ K and $B_c \sim 1$ T,

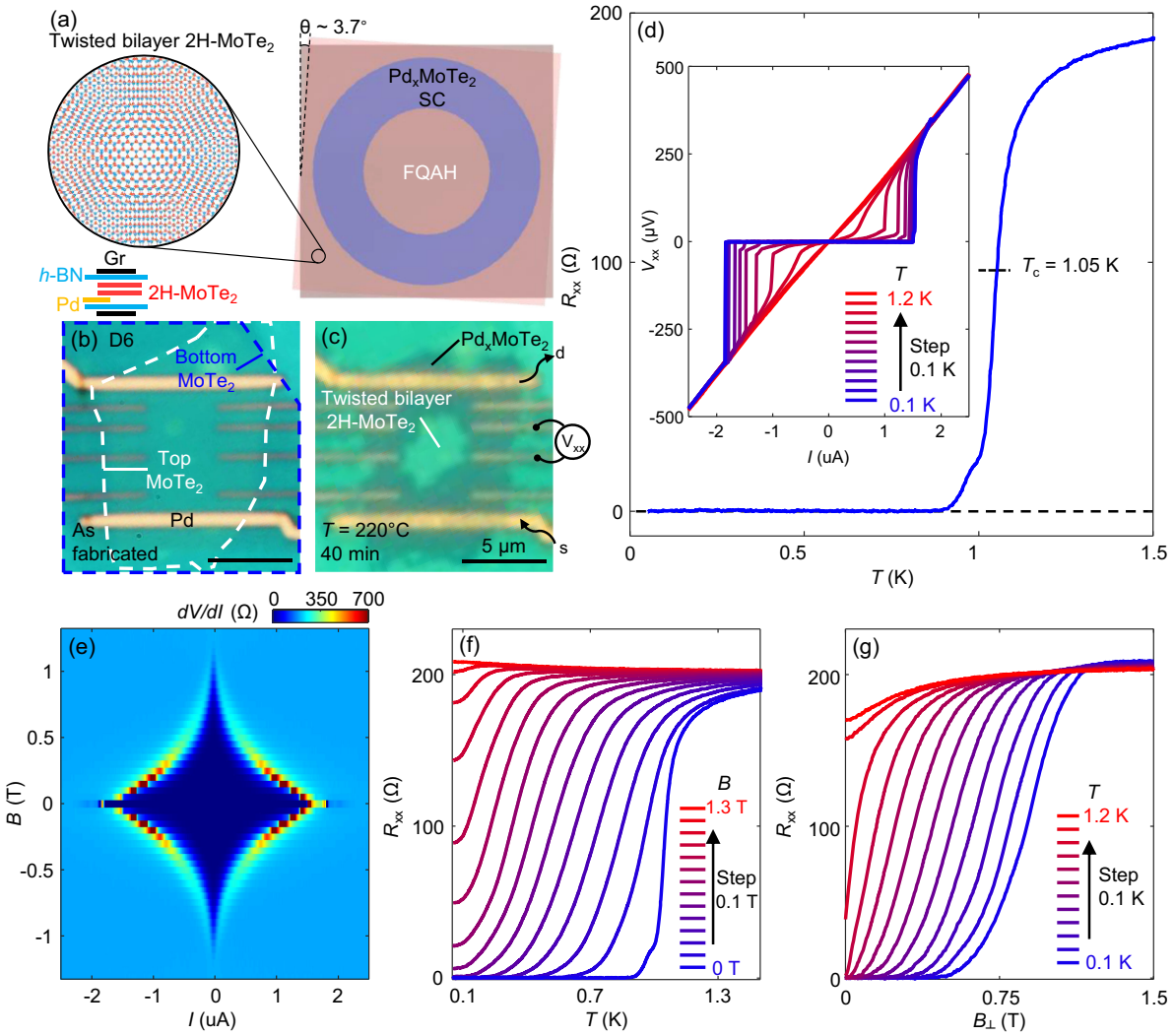

FIG. 4. Designing superconductivity in a fractional Chern insulator. (a) Top: an illustration of an in-plane heterojunction of a superconductor and a fractional Chern insulator realized in twisted bilayer 2H-$MoTe_2$. The moiré lattice is shown to the left. (b),(c) Optical images of a device (D6) consist of Pd stripes (electrodes) and twisted bilayer 2H-$MoTe_2$, fully encapsulated with graphite and *h*BN stacks, before (b) and after (c) the heat treatment. (d) R_{xx} versus T for Pd_xMoTe_2 realized in D6, revealing the superconducting transition. Inset shows the nonlinear IV curves taken at various T, displaying sharp jumps. The contact configuration used in the measurement is shown in (c). (e) A dV/dI map taken under varying B and I. (f) R_{xx} versus T taken under various B. (g) R_{xx} versus B taken at various T.

as characterized in Fig. 4). I_cR_n observed in this bilayer case is much larger than that of the monolayer seeded Pd compounds, indicating a larger superconducting gap, consistent with the higher T_c and B_c. In the Supplemental Material Fig. S6, we include data taken from the same device but under in-plane magnetic fields, in which superconductivity can survive >10 T, consistent the 2D nature of the superconductor [34].

We further note that the resistance transition of our Pd_xMTe_2 superconductors typically occurs within ~0.2 K. This is much sharper than, for example, the superconducting transition in magic-angle graphene [24], indicating a better homogeneity in our case. In some of our devices, a single I_c peak is seen [e.g., Figs. 2(e) and 4(e)], but others develop multiple peaks [e.g., Figs. 3(e) and 3(h)], suggesting that inhomogeneity in different devices is different, as expected. We in general find that Pd_xMTe_2 grown on bilayer MTe_2 exhibits a better uniformity than that grown on monolayers.

Our results establish a feasible device fabrication approach to study the interplay between superconductivity and FCIs in a highly designable fashion. In this device (D6), we have already realized a loop-shaped superconductor [Fig. 4(c)], the center of which is still intrinsic twisted bilayer 2H-$MoTe_2$ that can be gate tuned into FCIs. The properties of a device interfacing an FCI and a superconductor in a lateral junction are of interest to the construction and search of non-Abelian anyons.

We envision fruitful future explorations along this direction based on the approach and device presented here as well as their variations.

III. DISCUSSION

Beyond palladium, we have tested the phenomena on other metals. We do not find propagation of Au on WTe_2 at similar temperatures (Supplemental Material Fig. S7 [34]). We find Ni does propagate similarly on WTe_2, but the resulting new compound does not superconduct down to ~50 mK despite being metallic (Supplemental Material Fig. S8). The magnetic properties of the Ni-based compound, however, deserve further studies.

Our results establish a method of introducing superconductivity into a class of 2D topological chalcogenides. The rich topological phases and strong gate tunability of the host 2D materials distinguish our approach from the previous attempts in proximitizing epitaxy-grown topological insulators. The size and shape of the superconducting islands can be controlled via designing the pattern of Pd seeds and manipulating the recipes of the heat treatment. One key feature is that the heat treatment requires only a temperature as low as ~200 °C, which can be performed straightforwardly on a hot plate and/or under microscope. The whole process can be done inside a glovebox for devices on a chip without degrading the quality of sensitive components. We believe this unique approach for designing and creating robust superconductivity for air-sensitive 2D topological materials will enable a range of interesting explorations in condensed matter physics and superconducting quantum devices.

ACKNOWLEDGMENTS

This work is supported by AFOSR Young Investigator Award (No. FA9550-23-1-0140) to S. W. Electric transport measurement is partially supported by NSF through the Materials Research Science and Engineering Center (MRSEC) program of the National Science Foundation (DMR-2011750) through support to L. M. S. and S. W. and a CAREER Award (No. DMR-1942942) to S. W. Device fabrication is partially supported by ONR through a Young Investigator Award (No. N00014-21-1-2804) to S. W. S. W. and L. M. S. acknowledge support from the Eric and Wendy Schmidt Transformative Technology Fund at Princeton. S. W. acknowledges support from the Sloan Foundation. L. M. S. acknowledges support from the Gordon and Betty Moore Foundation through Grant No. GBMF9064 and the David and Lucile Packard Foundation and the Sloan Foundation. Y. J. acknowledges support from the Princeton Charlotte Elizabeth Procter Fellowship program. T. S. acknowledges support from the Princeton Physics Dicke Fellowship program. A. J. U. acknowledges support from the Rothschild Foundation and the Zuckerman Foundation. K. W. and T. T. acknowledge support from the JSPS KAKENHI (Grants No. 21H05233 and No. 23H02052) and World Premier International Research Center Initiative (WPI), MEXT, Japan.

[1] C. Nayak, S. H. Simon, A. Stern, M. Freedman, and S. Das Sarma, *Non-Abelian anyons and topological quantum computation*, Rev. Mod. Phys. **80**, 1083 (2008).
[2] J. Alicea and P. Fendley, *Topological phases with parafermions: Theory and Blueprints*, Annu. Rev. Condens. Matter Phys. **7**, 119 (2016).
[3] A. Yazdani, F. von Oppen, B. I. Halperin, and A. Yacoby, *Hunting for Majoranas*, Science **380** (2023).
[4] L. Fu and C. L. Kane, *Superconducting proximity effect and Majorana fermions at the surface of a topological insulator*, Phys. Rev. Lett. **100**, 096407 (2008).
[5] L. Fu and C. L. Kane, *Josephson current and noise at a superconductor/quantum-spin-Hall-insulator/superconductor junction*, Phys. Rev. B **79**, 161408(R) (2009).
[6] N. Read and E. Rezayi, *Beyond paired quantum Hall states: Parafermions and incompressible states in the first excited Landau level*, Phys. Rev. B **59**, 8084 (1999).
[7] N. H. Lindner, E. Berg, G. Refael, and A. Stern, *Fractionalizing Majorana fermions: Non-Abelian statistics on the edges of Abelian quantum Hall states*, Phys. Rev. X **2**, 041002 (2012).
[8] M. Cheng, *Superconducting proximity effect on the edge of fractional topological insulators*, Phys. Rev. B **86**, 195126 (2012).
[9] R. S. K. Mong, D. J. Clarke, J. Alicea, N. H. Lindner, P. Fendley, C. Nayak *et al.*, *Universal topological quantum computation from a superconductor-Abelian quantum Hall heterostructure*, Phys. Rev. X **4**, 011036 (2014).
[10] V. Mourik, K. Zuo, S. M. Frolov, S. R. Plissard, E. P. A. M. Bakkers, and L. P. Kouwenhoven, *Signatures of Majorana fermions in hybrid superconductor-semiconductor nanowire devices*, Science **336**, 1003 (2012).
[11] H. Ren, F. Pientka, S. Hart, A. T. Pierce, M. Kosowsky, L. Lunczer *et al.*, *Topological superconductivity in a phase-controlled Josephson junction*, Nature (London) **569**, 93 (2019).
[12] Ö. Gül, Y. Ronen, S. Y. Lee, H. Shapourian, J. Zauberman, Y. H. Lee *et al.*, *Andreev reflection in the fractional quantum Hall state*, Phys. Rev. X **12**, 021057 (2022).
[13] M. Endres, A. Kononov, M. Stiefel, M. Wyss, H. S. Arachchige, J. Yan, D. Mandrus, K. Watanabe, T. Taniguchi, and C. Schönenberger, *Transparent Josephson junctions in higher-order topological insulator* WTe_2 *via Pd diffusion*, Phys. Rev. Mater. **6**, L081201 (2022).
[14] M. Ohtomo, R. S. Deacon, M. Hosoda, N. Fushimi, H. Hosoi, M. D. Randle, M. Ohfuchi, K. Kawaguchi, K. Ishibashi, and S. Sato, *Josephson junctions of Weyl semimetal* WTe_2 *induced by spontaneous nucleation of* PdTe *superconductor*, Appl. Phys. Express **15**, 075003 (2022).
[15] Y. Wu, J. Zheng, Q. Li, M. Song, S. Yue, N. Lin, and L. Jiao, *Synthesis of superconducting two-dimensional non-layered* PdTe *by interfacial reactions*, Nat. Synthesis **1**, 908 (2022).

[16] J. T. Mlack, A. Rahman, G. Danda, N. Drichko, S. Friedensen, M. Drndić, and N. Marković, *Patterning superconductivity in a topological insulator*, ACS Nano **11**, 5873 (2017).

[17] M. D. Randle, M. Hosoda, R. S. Deacon, M. Ohtomo, P. Zellekens, K. Watanabe *et al.*, *Gate-defined Josephson weak-links in monolayer* WTe_2, Adv. Mater. **35** (2023).

[18] M. Bai, F. Yang, M. Luysberg, J. Feng, A. Bliesener, G. Lippertz, A. A. Taskin, J. Mayer, and Y. Ando, *Novel self-epitaxy for inducing superconductivity in the topological insulator* $(Bi_{1-x}Sb_x)_2Te_3$, Phys. Rev. Mater. **4**, 094801 (2020).

[19] M. Bai, X.-K. Wei, J. Feng, M. Luysberg, A. Bliesener, G. Lippertz, A. Uday, A. A. Taskin, J. Mayer, and Y. Ando, *Proximity-induced superconductivity in* $(Bi_{1-x}Sb_x)_2Te_3$ *topological-insulator nanowires*, Commun. Mater., **3**, 20 (2022).

[20] X.-K. Wei, A. R. Jalil, P. Rüßmann, Y. Ando, D. Grützmacher, S. Blügel, and J. Mayer, *Atomic diffusion-induced polarization and superconductivity in topological insulator-based heterostructures*, ACS Nano **18**, 571 (2024).

[21] I. T. Rosen, C. J. Trimble, M. P. Andersen, E. Mikheev, Y. Li, Y. Liu *et al.*, *Fractional ac Josephson effect in a topological insulator proximitized by a self-formed superconductor*, arXiv:2110.01039.

[22] V. Fatemi, S. Wu, Y. Cao, L. Bretheau, Q. D. Gibson, K. Watanabe, T. Taniguchi, R. J. Cava, and P. Jarillo-Herrero, *Electrically tunable low-density superconductivity in a monolayer topological insulator*, Science **362**, 926 (2018).

[23] E. Sajadi, T. Palomaki, Z. Fei, W. Zhao, P. Bement, C. Olsen, S. Luescher, X. Xu, J. A. Folk, and D. H. Cobden, *Gate-induced superconductivity in a monolayer topological insulator*, Science **362**, 922 (2018).

[24] Y. Cao, V. Fatemi, S. Fang, K. Watanabe, T. Taniguchi, E. Kaxiras, and P. Jarillo-Herrero, *Unconventional superconductivity in magic-angle graphene superlattices*, Nature (London) **556**, 43 (2018).

[25] J. M. Park, Y. Cao, K. Watanabe, T. Taniguchi, and P. Jarillo-Herrero, *Tunable strongly coupled superconductivity in magic-angle twisted trilayer graphene*, Nature (London) **590**, 249 (2021).

[26] J. M. Park, Y. Cao, L.-Q. Xia, S. Sun, K. Watanabe, T. Taniguchi, and P. Jarillo-Herrero, *Robust superconductivity in magic-angle multilayer graphene family*, Nat. Mater. **21**, 877 (2022).

[27] Y. Jia, F. Yuan, G. Cheng, Y. Tang, G. Yu, T. Song *et al.*, *Surface-confined two-dimensional mass transport and crystal growth on monolayer materials*, Nat. Synthesis **3**, 386 (2024).

[28] X. Qian, J. Liu, L. Fu, and J. Li, *Quantum spin Hall effect in two-dimensional transition metal dichalcogenides*, Science **346**, 1344 (2014).

[29] Z. Fei, T. Palomaki, S. Wu, W. Zhao, X. Cai, B. Sun, P. Nguyen, J. Finney, X. Xu, and D. H. Cobden, *Edge conduction in monolayer* WTe_2, Nat. Phys. **13**, 677 (2017).

[30] S. Wu, V. Fatemi, Q. D. Gibson, K. Watanabe, T. Taniguchi, R. J. Cava, and P. Jarillo-Herrero, *Observation of the quantum spin Hall effect up to 100 kelvin in a monolayer crystal*, Science **359**, 76 (2018).

[31] P. Wang, G. Yu, Y. Jia, M. Onyszczak, F. A. Cevallos, S. Lei *et al.*, *Landau quantization and highly mobile fermions in an insulator*, Nature (London) **589**, 225 (2021).

[32] Y. Jia, P. Wang, C. Chiu, Z. Song, G. Yu, B. Jäck *et al.*, *Evidence for a monolayer excitonic insulator*, Nat. Phys. **18**, 87 (2022).

[33] B. Sun, W. Zhao, T. Palomaki, Z. Fei, E. Runburg, P. Malinowski *et al.*, *Evidence for equilibrium exciton condensation in monolayer* WTe_2, Nat. Phys. **18**, 94 (2022).

[34] See Supplemental Material at http://link.aps.org/supplemental/10.1103/PhysRevX.14.021051 for device fabrication details, transport measurement setups as well as more supplemental data.

[35] Y. Qi, P. G. Naumov, M. N. Ali, C. R. Rajamathi, W. Schnelle, O. Barkalov *et al.*, *Superconductivity in Weyl semimetal candidate* $MoTe_2$, Nat. Commun. **7**, 11038 (2016).

[36] W. Wang, S. Kim, M. Liu, F. A. Cevallos, R. J. Cava, and N. P. Ong, *Evidence for an edge supercurrent in the Weyl superconductor* $MoTe_2$, Science **368**, 534 (2020).

[37] E. Anderson, F.-R. Fan, J. Cai, W. Holtzmann, T. Taniguchi, K. Watanabe, D. Xiao, W. Yao, and X. Xu, *Programming correlated magnetic states with gate-controlled moiré geometry*, Science **381**, 325 (2023).

[38] J. Cai, E. Anderson, C. Wang, X. Zhang, X. Liu, W. Holtzmann *et al.*, *Signatures of fractional quantum anomalous Hall states in twisted* $MoTe_2$, Nature (London) **622**, 63 (2023).

[39] H. Park, J. Cai, E. Anderson, Y. Zhang, J. Zhu, X. Liu *et al.*, *Observation of fractionally quantized anomalous Hall effect*, Nature (London) **622**, 74 (2023).

[40] Y. Zeng, Z. Xia, K. Kang, J. Zhu, P. Knüppel, C. Vaswani, K. Watanabe, T. Taniguchi, K. F. Mak, and J. Shan, *Thermodynamic evidence of fractional Chern insulator in moiré* $MoTe_2$, Nature (London) **622**, 69 (2023).

[41] F. Xu, Z. Sun, T. Jia, C. Liu, C. Xu, C. Li, Y. Gu, K. Watanabe, T. Taniguchi, B. Tong *et al.*, *Observation of integer and fractional quantum anomalous Hall effects in twisted bilayer* $MoTe_2$, Phys. Rev. X **13**, 031037 (2023).